Road Segmentation using Multipass Single-Pol Synthetic Aperture Radar Imagery[1]

Mark W. Koch, Mary M. Moya, Jim G. Chow, Jeremy Goold, and Rebecca Malinas
Sandia National Laboratories[2]
Albuquerque, NM 87185-1163
mwkoch@sandia.gov

Abstract

Synthetic aperture radar (SAR) is a remote sensing technology that can truly operate 24/7. It's an all-weather system that can operate at any time except in the most extreme conditions. By making multiple passes over a wide area, a SAR can provide surveillance over a long time period. For high level processing it is convenient to segment and classify the SAR images into objects that identify various terrains and man-made structures that we call "static features." In this paper we concentrate on automatic road segmentation. This not only serves as a surrogate for finding other static features, but road detection in of itself is important for aligning SAR images with other data sources. In this paper we introduce a novel SAR image product that captures how different regions decorrelate at different rates. We also show how a modified Kolmogorov-Smirnov test can be used to model the static features even when the independent observation assumption is violated.

1. Introduction and problem

Synthetic aperture radar (SAR) [23] is a remote sensing technology that can truly operate 24/7. It's an all-weather system that can image at any time except in the most extreme conditions. It can operate either day or night and has a long standoff. SAR combines multiple results from different viewing angles to create a high resolution image of an area. For the area it is illuminating, SAR is a coherent imager that measures both phase and magnitude of the return. Using two registered images taken at different times, one can use coherent change detection (CCD) [23] to detect minute changes from one collection to the next.

By making multiple passes over a wide area, a SAR can provide surveillance for long time periods. One research area of interest is exploiting this large amount of imagery to learn about activities in the surveillance area. One approach uses a geospatial-temporal semantic graph [4]. Here nodes of the graph represent fundamental objects in the image data such as buildings, road, water, etc., and the edges represent their spatial and temporal relationships. Image searches such as "find all the buildings >200m from a paved road," can then be accomplished using the graph framework.

Before a geospatial-temporal semantic graph can ingest this large amount of data, it is necessary to segment and classify the SAR images into objects that identify various terrains and man-made structures. Here, we refer to these objects as *static-features*.

In this paper we concentrate on the detection and classification of roads in SAR images. Road detection not only serves as a surrogate for finding other static features, but it is in of itself important for aligning SAR images with other data sources such as maps, light detection and ranging (LIDAR) images, or optical imagery.

In this paper we also concentrate on single-pol SAR imagery. While fully-polarimetric SAR can be decomposed into scattering mechanisms [7][8][11][32][33][49][57] and is very helpful in static feature extraction, many current SAR systems in use only have a single polarization. If multiple polarizations are available, our approach can be extended to incorporate the additional polarimetric information.

2. Previous work on road finding in SAR

Road detection in SAR imagery has applications in route mapping for emergency vehicles and alignment of spatial datasets. In recent years, approaches to both semi-automated and automated SAR road detection have been considered. Semi-automatic approaches [5][6][25][28][29][58][60] for high-resolution images gained traction for the following reasons: complexity and variability of road characteristics, road discontinuities caused by shadows, layover [23], and isolated bright areas, and ambiguity in terrain with similar characteristics to roads. These semi-automatic approaches generally assume or explicitly

[1] This work was supported by PANTHER, a Laboratory Directed Research and Development (LDRD) Project at Sandia National Laboratories. For additional information about PANTHER, please contact Kristina Czuchlewski, Ph.D., krczuch@sandia.gov.

[2] Sandia is a multiprogram laboratory operated by Sandia Corporation, a Lockheed Martin Company, for the United States Department of Energy's National Nuclear Security Administration under Contract DE-AC04-94AL85000. SAND#2014-2731C

model certain road characteristics such as low intensity, elongated shape, low curvature, constant width. Most methods follow a two-step process: a local detection step to identify likely road segments in an image followed by a global optimization step to join candidate segments while suppressing false alarms. The detector parameters are derived from a user-defined road center-point or road segment in the image. Cheng *et al*. [6] proposes local road segment detection using a double-window template followed by a global particle filtering step. This method requires a user-input road center-point for the template, and additional seed points in the event of tracker failure. Zhou [60] proposes a human-computer interaction system for road tracking in which a user sets an initial state for a Bayesian filter, as well as providing seed points in the event of tracker failure. An earlier work by Kim *et al*. [25] detects road segments based on least-squares correlation matching, thereby avoiding a global tracking step, and also requires a user-given road center-point for the matching step. In these approaches, tracking is typically interrupted by shadows, layover, isolated bright points, or abrupt changes in intensity along roads. Resolution of 1m is considered high, and road detection is based on a single SAR image of a scene.

Many automated methods [1][19][20][21][24][30][36][39][41][42][54] also take a local detection-global optimization approach, often including a speckle reduction step. Detection is generally performed using single SAR images, although occasionally multi-aspect data is used. Many of these methods perform the detection-optimization based on a priori knowledge of road geometries or context objects, in addition to road intensity characteristics. Amberg *et. al* [1] and Wessel [54] take a context-based approach to automatic local detection and global optimization. Context based approaches weight detected road segments according to the existence of nearby context objects, such as vehicles or building layover, that likely indicate roads. These weights can be incorporated into the cost function for optimization or as a post-processing step to optimally join disjoint road segments and reject false alarms. Jeon *et. al* [24] models roads as curvilinear, finite-width structures. After speckle reduction and applying a threshold, they extract curve segments and optimally group the segments using perceptual grouping factors. Noisy curve segments are removed prior to the grouping procedure. Negri *et. al* [39] recovers road networks using junction-preserving segment detection followed by a Markov random field network optimization step, where the likelihood term is based on a priori knowledge that roads must pass through junctions. This work was tested on both 5m and .5m resolution full-polarization images. On the .5m resolution test image, 64% correctness and 77% completeness were reported. In a related work, Lisini *et. al* [30] proposes a fusion of road networks recovered at multiple resolutions from a local detection-global optimization procedure. Both segment detection and network optimization are based on the fusion of a curvilinear detector and intensity classification map. Network optimization is performed via Markov random fields with likelihood term based on the detector-classification fusion output. This method was tested on 1.25m and sub-meter resolution images. The sub-meter resolution image demonstrated 78% correctness and 46% completeness. More recently, other multi-resolution approaches have been considered for the candidate segment grouping/network optimization step. He *et. al* [19] uses multiscale geometric analysis to perform the candidate segment grouping step after a local detection process, and Perciano et. al [41] uses a hierarchical Markov random field for network optimization, following detection via fusion of ratio- and correlation-based line detectors. Finally, Hedman and Hinz [20] adapted the local detection-network optimization approach to multi-aspect SAR data via Bayesian network fusion.

Other recent road detection approaches have included scene classification based on spatial context [42] and adaptive region growing [36]. Popescu *et. al* [42] classify scenes, such as those containing roads, using a set of spectral features derived from large image patches that provide spatial context. These features can discriminate between approximately 30 scene classes with a recognition rate of at least 50% for 1m resolution imagery. In Lu *et. al* [36], adaptive region growing in the global optimization step achieved a reported 86% correctness and 56% completeness in road detection in a .5m resolution image.

In contrast to the above automatic methods, our approach uses statistics of multi-pass, high resolution SAR products taken over a long time period. A novel SAR product is developed called a long-term CCD (LCCD) image which indicates that man-made objects decorrelate slowly over time in comparison to natural features. Combining the LCCD with a time-averaged backscatter product provides high-confidence road detection. Following an offline training phase, our approach is fully-automated with high probability of correct detection.

Our approach is unique in that it not only makes use of higher-resolution and multiple SAR products, but takes advantage of the fact that paved roads tend to decorrelate slowly over time. The classification algorithm is based on probabilistic fusion that produces a goodness-of-fit test statistic, which creates closed decision boundaries that surround classes-off-interest represented by the training set. It also excludes samples dissimilar to anything in the training set by declaring them as an "unknown" class. The input to the fusion algorithm is based on the Kolmogorov-Smirnov (KS) test. Unfortunately, the SAR products violate the independence assumption required for the KS test. We also introduce a novel way for handling this by using training data to modify the null distribution for the

KS test. We reserve enforcing contextual and shape constraint for higher levels of processing.

3. Overall approach

Figure 1 shows a block diagram for our approach. The input is based on what we call *SAR image products*. These products result from combining SAR images from multiple passes. Here we assume the images have been calibrated and are collected at approximately the same aspect and grazing angles. For example by registering multiple SAR images of the same area collected at different times, one can reduce speckle (described in section 4) and Doppler streaks by using the median value of each pixel across the time dimension. This produces cleaner images while maintaining spatial resolution.

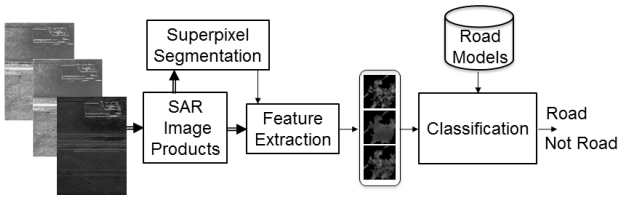

Figure 1: Block diagram of SAR road detection approach.

Next a superpixel segmentation algorithm is used to group pixels into homogeneous regions. For each superpixel, feature extraction involves identifying corresponding pixels in each SAR product. In the classification stage statistical models of roads for each image product is matched to the corresponding feature vector. The feature vectors are then combined using probabilistic fusion.

4. SAR speckle

SAR speckle is an artifact of coherent imaging. In the magnitude domain, speckle for a region with constant backscatter is typically modeled with a Rayleigh distribution [52]:

$$f(x) = (x/b^2)\exp(-x^2/(2b^2)) \quad (1)$$

where x is a random variable that represents the SAR return in a pixel in the magnitude domain and b represents the scale parameter. The mean and variance of the Raleigh is $\mu = b\sqrt{\pi/2}$ and $\sigma^2 = (2-\pi/2)b^2$ respectively. Here, as the mean of backscatter increases so does the variance.

Lee [33] has shown that histograms of SAR images are unimodal even if they contain multiple regions with different backscatter means. For example, Figure 2a shows a SAR image with both paved and dirt road regions, high desert scrub region, and a building region, but the probability density function (Figure 2b) is unimodal. Lee [33] has shown that a subaperture multilook approach makes it easier to separate regions with different mean backscatter.

Approaches using gradients, which are popular in optical image processing, are also problematic in SAR because of the speckle. Gradient approaches which assume additive Gaussian noise tend to emphasize the SAR speckle. Figure 3a shows a 128x128 chip of a homogeneous region from the image in Figure 2. The coefficient of variation σ/μ for the chip in the magnitude domain is 0.54. For a Rayleigh distribution, this value is close to the theoretical value of $\sqrt{4\pi - 1}$ (~0.52). If one applies a Canny edge detector to the entire image and uses parameters that would eliminate all but the strongest edges in an optical image one can see edges created by the speckle. These edges appear in a homogeneous region where there should be no edges. This is also apparent in CCD images, for example see Figure 4. In summary, current optical techniques can't be arbitrarily applied and may not extend well, or may need to be modified for SAR imagery.

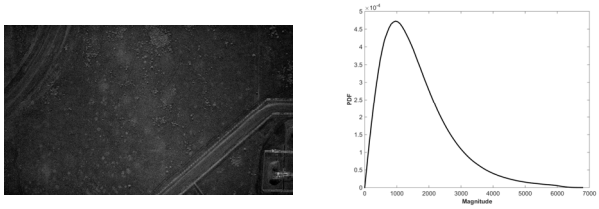

(a) (b)

Figure 2: Example SAR image and its corresponding PDF.

To avoid these problems researchers often use speckle reduction algorithms. Similar to image morphology, the Crimmins algorithm [10] uses an iterative geometric approach for reducing clutter. A comparison article [16] discusses some of the most popular speckle reduction approaches [14][27][31] and compares them to wavelet approaches. Like any smoothing approach there is a tradeoff in reducing speckle and keeping fine features, but it does allow the application of optical type algorithms.

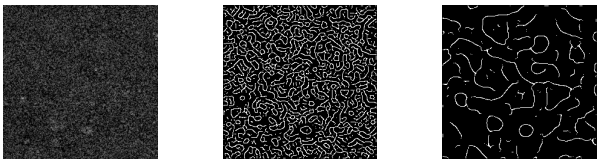

(a) (b) (c)

Figure 3: Edge detection on a SAR image for a homogeneous area. (a) SAR homogenous region. (b) Canny edge detector with $\sigma = 3$. (c) $\sigma = 6$.

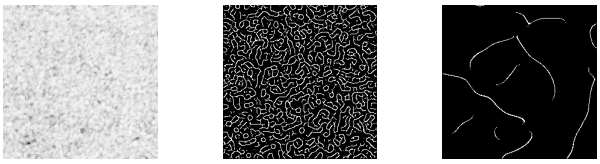

(a) (b) (c)

Figure 4: Edge detection on a SAR image for a homogeneous area. (a) CCD image from a homogeneous region. (b) Canny edge detector with $\sigma = 3$. (c) $\sigma = 6$.

5. Multipass SAR image products

By exploiting temporal and spatial statistics it is possible to derive a number of SAR image products designed to reduce speckle without reducing the effective resolution.

5.1. Subaperture multilook

As suggested by the work of Lee [33] we create a subaperture multilook image [23] which is used by the superpixel oversegmentation algorithm. Forming a subaperture multilook image requires transforming a complex-valued SAR image back to the two-dimensional Fourier domain, partitioning the spectrum into non-overlapping pieces and non-coherently averaging the images formed from each piece of the spectrum [15]. The subaperture multilook image has coarser spatial resolution than an SAR backscatter magnitude image formed from the complete phase history, but also has reduced speckle. See Figure 5b for a four-look subaperature multilook and Figure 5a for the corresponding SAR image.

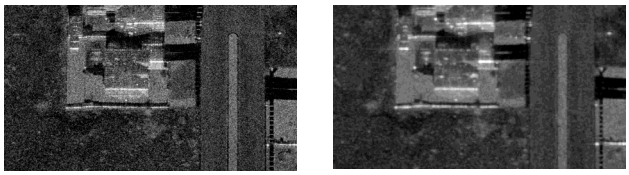

(a) (b)

Figure 5: Example SAR and multilook images. (a) Calibrated SAR image. (b) Four look subaperature multilook.

5.2. Median over time radar cross section (RCS) image

We can use multiple passes of SAR images collected from the same scene to compute image statistics for speckle reduction. We calibrate each radar cross section (RCS) image and, from a stack of co-registered RCS images of the same scene, compute a median image to form the median-RCS image, which is a temporal multilook product. Figure 6a shows an example of an median RCS image.

5.3. Long term CCD image

We define a long-term CCD (LCCD) image as a CCD image where the time elapsed between the first SAR image and the second SAR image is greater than a single day. In order to understand the overall decorrelation as time increases, LCCDs were generated for increasing time delta's from $\Delta t = 1 \text{ to } 14$ days. For each time delta, multiple LCCDs are possible. For example, a $\Delta t = 2$ LCCD can be generated for SAR images collected on March 1st and March 3rd. A $\Delta t = 2$ LCCD could also be generated for SAR images collected on March 2nd and March 4th.

Once LCCDs are generated for a specific Δt, the resulting LCCDs are co-registered into an image stack. The median LCCD is then calculated for a Δt by finding the median value for each pixel from all corresponding pixels in the stack. The result is a single median-LCCD image for the given time delta. The median helps remove Doppler streaks that can appear in SAR images because of moving vehicles and minor weather disturbances. Figure 6b shows an example of a median LCCD image from the same scene as in Figure 5a.

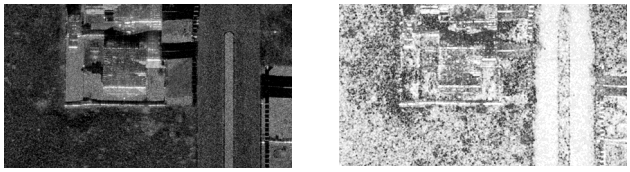

(a) (b)

Figure 6: Example SAR product images. (a) Median RCS (b) Median-LCCD for Δt =14 days

To analyze the behavior of the LCCD for different static features, analysts selected representative superpixels for each statistic feature. The plots in Figure 7 show the result of taking the mean of the median-LCCD values for these superpixels and plotting how the mean changes with Δt. The Figure shows that at $\Delta t = 1$, there are basically three ranges of LCCD values: high, medium, and low. High LCCD is around 0.9 and occurs for paved-roads, gravel, and desert static-features. Low LCCD is below 0.5 and occurs for shadows and trees. Here the pixels are essentially decorrelated. Medium LCCD occurs between 0.8 and 0.6. The static-features in this range are man-made, cement, and soil. As Δt increases soil and desert decorrelate at a high rate whereas paved, man-made, gravel and cement decorrelate at a much slower rate. This type of feature is very powerful in discriminating paved-road from hard packed soil. Here both have similar RCS, but the soil decorrelates faster.

6. SAR segmentation

Image segmentation is the process of dividing an image into homogeneous regions. Instead of classifying individual pixels or using sliding-window-processing of pixels, we segment the image into superpixels. A wide body of research has been developed for, and have applied, superpixel algorithms for optical imagery [15][1][44][35]. In our work these superpixels form groups of approximately 500 pixels that have similar location and intensity. They facilitate statistical characterization of classes by providing self-similar regions, reducing computation complexity, and following natural boundaries instead of introducing artifacts as sliding window approaches often do.

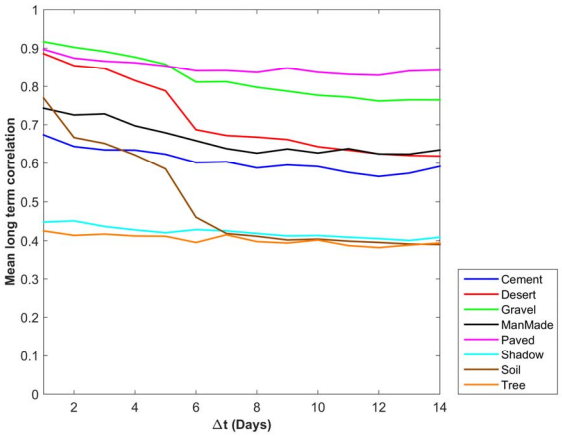

Figure 7: Mean LCCD for $\Delta t = 1$ to 14 days and different types of static-features (best viewed in color).

Recent works [51][55][17][59][56][38] have allowed application of superpixel segmentation to SAR imagery, as well, in spite of SAR speckle. We follow the approach of [38] and use the Simple Linear Iterative Clustering (SLIC) algorithm. The SLIC algorithm implements a localized *k*-means [37][12] algorithm with a Euclidean distance metric that depends on both spatial and intensity differences. When applying SLIC to an RCS domain such as subaperture multilook, we use the log-magnitude domain. Here, Euclidean distance in the log-magnitude domain is equivalent to a ratio-intensity distance in the magnitude domain, as proposed by Xiang *et. al* [56].

Achanta, et.al. [1] use the LAB color space channels, with equal weights when applying SLIC to optical color imagery. We may select one, two or three of the coregistered SAR image products as input channels for the SLIC segmentation. If we had reason to believe that any channel(s) were more important than other(s), we could weight the images accordingly. Figure 8 shows an example of a superpixel segmentation using the subaperture multilook SAR image in Figure 5b.

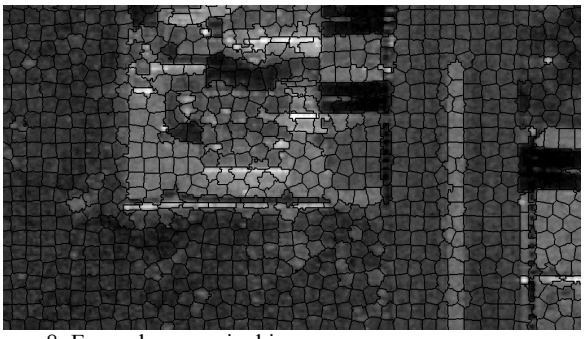

Figure 8: Example superpixel image.

7. Classification

Figure 9 shows the classification approach in more detail. The core of the approach is what we call a *match matrix*. Each row of the match matrix represents a superpixel from a SAR image product. Each column represents models for a static-feature of interest. In this paper, the columns represent different types of pavements in roads. Each entry in the match matrix represents the score of matching the appropriate model to the superpixel corresponding to the correct SAR image product. Sensor fusion then combines the scores together and the classification module selects the best score from the different fusion algorithms.

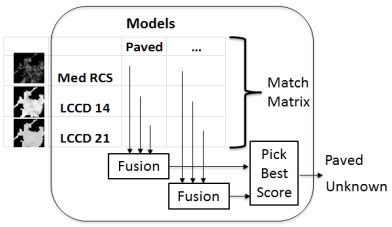

Figure 9: Classification approach.

7.1. Train, test and validation data

Our approach is a supervised training approach, where for each model of interest, we identify approximately 300 superpixels. One third of the superpixels are used for training, one third for test, and one third for validation. The superpixels are selected to be roughly homogeneous in content with consistent radar parameters: frequency, polarization, and grazing angle.

7.2. Kolmogorov-Smirnov test

As discussed in Section 4 the Rayleigh distribution is a good model for SAR backscatter from homogenous clutter regions such as bare ground, dense forest canopies, and snow covered ground [52]. For nonhomgenous regions other models have been proposed. For example, the lognormal or Weibull distributions have been used for sea ice [52]. Salazar proposed using the beta prime distribution as a unified model for describing homogeneous and heterogeneous clutter and extremely

heterogeneous (man-made) areas [46][47]. The beta prime model is completely characterized by two parameters, which dictate the shape and scale of the SAR data. Unfortunately, estimating shape and scale parameters doesn't have a closed form solution. In [18] Gao gives a summary of the 40 year history of SAR modeling and gives more than a 100 references on the subject.

A parametric test would not only require estimating the parameters of the distribution, but to have knowledge of the form of the distribution. This can be problematic for large numbers of SAR image products and static-features.

Instead of using a parametric model to describe superpixels for different static-features and SAR image products, we use the nonparameteric two sample Kolmogorov-Smirnov (KS) test [26][50][43]. The training process creates a nonparametric cumulative distribution function (CDF) for each SAR image product associated with each static-feature. The KS test compares the CDF of pixels within a test superpixel against each trained CDF and produces a match statistic for each. This allows the algorithm to adapt to any distribution for a given static-feature and SAR image-product.

Let $F_n(x)$ represent an empirical CDF defined by n observations from an independent and identically distributed (*iid*) sample $X_1,\ldots X_n$ under a superpixel. Then

$$F_n(x)=\frac{1}{n}\sum_{i=1}^{n} I(X_i<x) \tag{2}$$

where the indicator function $I(X_i<x)$ is 1 if $X_i<x$ and 0 otherwise. Suppose the empirical CDF from the training data is represented by $G_m(x)$ then the two-sample KS test for testing the hypotheses

$$H_0: F=G \quad \text{vs.} \quad H_1: F\neq G \tag{3}$$

is

$$D_{nm}(x)=\sqrt{K}\sup_x |F_n(x)-G_m(x)| \tag{4}$$

where $K=mn/(n+m)$. For the null hypothesis H_0:

$$\Pr(D_{nm}(x)<t)\rightarrow H(t)=1-2\sum_{i=1}^{\infty}(-1)^{i-1}e^{-2i^2t} \tag{5}$$

Let μ_H and σ_H^2 represent the mean and variance of $H(t)$ respectively. Then

$$\mu_H=\sqrt{\pi/2}\ln(2) \text{ and } \sigma_H^2=\pi/12-\mu^2. \tag{6}$$

The KS test is attractive, because the p-value for the null hypothesis can be estimated and used for the probabilistic fusion algorithm (Section 7.3). Unfortunately, the observations $X_1,\ldots X_n$ are not independent for the SAR image products. To handle this we take the approach of Bayley [3]. Here we estimate how the effective number of observations affects the mean and variance of $H(t)$ using the training data and a leave-one-out (LOO) method. Our approach is inspired by the work of Zhang and Wu [60] who use a beta distribution to approximate the distribution of the KS statistic $H(t)$ for an *iid* sample. The approximation is given by the following equation:

$$H(t)\sim aB_{p,q}+b \tag{7}$$

where $B_{p,q}$ is the beta distribution with parameters $p,q>0$, and the parameters a,b scale and shift the beta distribution respectively. The four constants a,b,p,q are selected so that the first four moments of $H(t)$ match those of $aB_{p,q}+b$. Zhang and Wu show the approximation is very simple and accurate.

Instead of a beta distribution we use $H(t)$ itself and the parameters a,b to create a new distribution $\tilde{H}(t)$ that can handle the nonindependence of the superpixel sample. This is given by the following equation:

$$H(t)\sim a\tilde{H}(t)+b \tag{8}$$

The parameters a,b are selected so that the mean and variance of $\tilde{H}(t)$ matches the mean and variance of $H(t)$ given by equation (6). Thus

$$a=\sigma_{H(t)}/\sigma_{\tilde{H}(t)} \text{ and } b=u_{H(t)}-au_{\tilde{H}(t)} \tag{9}$$

where $\mu_{\tilde{H}(t)}$ and $\sigma^2_{\tilde{H}(t)}$ represent the mean and variance of $\tilde{H}(t)$, respectively. Here $\mu_{\tilde{H}(t)}$ and $\sigma^2_{\tilde{H}(t)}$ are empirically estimated using the superpixel training data and a LOO technique. The superpixels that belong to the class of interest can have different sizes and shapes. The key assumption, based on Bayley's work, is that nonindependence affects the effective number of independent observations and thus only the mean and variance of the distribution $H(t)$.

Figure 10 shows the result of this approach for the paved road static-feature class using the median RCS image product. From the *N* training superpixels *N-1* are selected to create a model $G_m(x)$ where *m* is the total number of pixels in the *N-1* superpixels. Assuming the left-out superpixel has *n* pixels then we can compute $F_n(x)$ and $D_{nm}(x)$. We can now compute *N* such scores. In the Figure the red curve shows the distribution of these scores using a Parzen kernel density estimator [40][12]. Because of the violation of the independence assumption, the distribution doesn't match the theoretical $H(t)$ shown by the dotted black curve. Using equation (9) we create a new distribution shown by the blue curve that gives a much closer approximation to the true distribution.

7.3. Probabilistic fusion

From Figure 9 it can be seen that the goal of fusion is to combine the match scores for each static feature. The important steps in this process are to normalize the scores

so they can be easily combined and account for any dependence between the scores. To accomplish this we use probabilistic fusion [48].

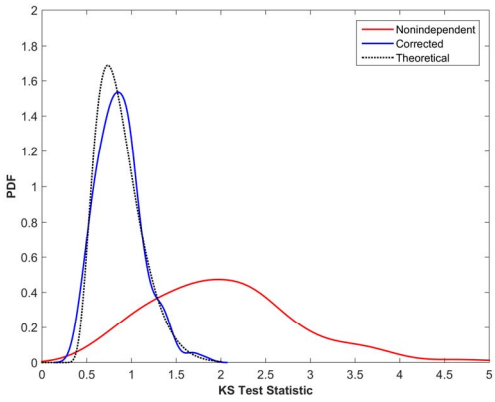

Figure 10: Corrected $H(t)$ to account for the nonindependence of the sample underneath a superpixel (best viewed in color).

Let $t_{i,j}$ represent a KS test score (4) in the match matrix where i represents an index into the SAR image product and j represents the static feature. For ease of presentation we will drop the j and use t_i, $i=1,\ldots,p$ to represent the scores to fuse. After the nonindependence correction (9) and assuming the null hypothesis is true, $H(t_i)$ is the CDF of t_i and $1-H(t_i)$ is the p-value and is uniformly distributed [22]. It follows that

$$Y_i = -\log(1-H(t_i)) \tag{10}$$

is exponentially distributed [13]. It is expected that Y_i will be large for superpixels that violate the null hypothesis. This process normalizes the KS scores so that they can be combined for different products by simple addition:

$$S_f = \sum_{i=1}^{p} Y_i \tag{11}$$

where S_f is the fused score. The distribution of S_f is approximated as a gamma for the null distribution with parameters

$$\hat{r} = \frac{p^2}{p+C}, \text{ and } \hat{\lambda} = \frac{p}{p+C} \tag{12}$$

where $\hat{r}$ and $\hat{\lambda}$ are the shape and scale parameters of the gamma distribution respectively, $C = \sum_{i=1}^{N}\sum_{j\neq i}\hat{\rho}_{ij}$, and $\hat{\rho}_{ij}$ represent the estimated correlation between Y_i and Y_j. The correlation coefficients $\hat{\rho}_{ij}$ are estimated from labeled training data. See the reference [48] for more details.

Because each Y_i is expected to be large for superpixels that violate the null hypothesis, it is sensible to make the corresponding static feature identification decisions by setting a threshold on the value of S_f. Fused scores at or below the chosen threshold are classified as the corresponding static features, while those with scores above the threshold are classified as unknown.

8. Results

For training, test, and validation data we select approximately 300 superpixels of the following static-features: paved road, shadow, man-made (dihedral and trihedral returns), scrub desert, bare earth, gravel, cement, and trees. One third of the data is used for training and developing KS models of paved roads, one third for tests and parameter selection and one third for validation. Probabilistic fusion is a goodness-of-fit approach so we only need to develop models of the paved road class. All other classes should have large fused scores indicating an unknown (nonpaved) class. For paved-road, the distribution of fused scores should follow a gamma distribution with parameters $\hat{r}$ and $\hat{\lambda}$ (12).

Figure 11 shows the receiver operating characteristic (ROC) curves using the test data. Here we plot the probability of false alarm (PFA) vs. probability of detection (PD). Each point on the ROC is determined by a threshold τ_f on the fused score S_f. The decision is given by the following:

Figure 11a shows the ROC curve when using just the score from the KS test of the paved road template for the median-RCS SAR product. Figure 11b shows the result using the median-LCCD with $\Delta t = 14$ days and Figure 11c shows the result using the median-LCCD $\Delta t = 21$ days. Finally Figure 11d shows the result of using probabilistic fusion and it should be readily apparent that probabilistic fusion significantly improves the results.

Figure 12b shows an example of the paved superpixels dectected from the SAR image in Figure 12a. Yellow indicate superpixels that were labeled as paved and black indicates superpixels labeled as unknown.

Figure 13 shows the road labeled on a larger SAR strip of approximately 0.1 km^2. One can see the road is well defined and there are some minor isolated false alarms in the scrub desert area. These false alarms are mostly likely caused by hard packed soil in the scrub desert area.

In future work we will use a conditional random field with the superpixels as the nodes [15] that will enforce spatial consistency constraints to remove these isolated superpixels.

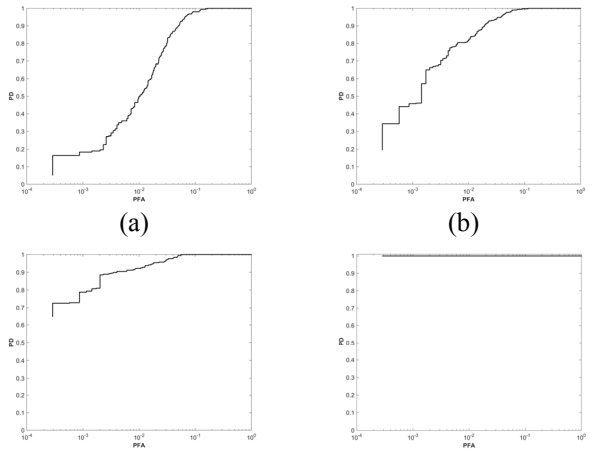

(a) (b) (c) (d)

Figure 11: Performance results on a small set of training data. ROC curves plot the PFA vs PD for various decision threshold. (a) Median RCS. (b) LCCD with $\Delta t = 14$. (c) LCCD with $\Delta t = 21$. (d) Probabilistic fusion using all three SAR products.

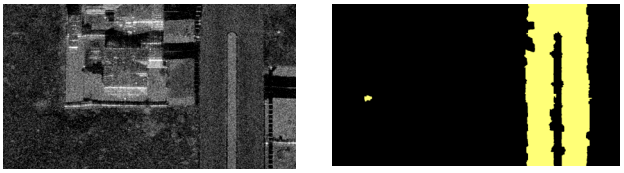

(a) (b)

Figure 12: Example output. (a) SAR image. (b) Superpixels identified as paved road. Yellow indicates paved road and black indicates the unknown class (best viewed in color).

9. Conclusion

With the availability of a large amount of high resolution surveillance data we have a unique opportunity to build on current approaches and find new ways to segment SAR images, specifically automatically identifying paved-roads in SAR imagery. The phenomenon of SAR speckle requires careful consideration on using standard optical approaches for image segmentation. With the availability of a long time history of SAR imagery for a specific area, we have introduced a new SAR product based on a long term CCD. Usually the time separation between successive SAR collections for a CCD creation is on the order of hours, but we have investigated how different regions decorrelate over many days. We have found that the type of terrain often determines the rate of decorrelation. Here, the paved-road static feature maintains a high degree of coherence even after many days. Even with LCCD images there is still a large amount of confusion between certain high desert areas, man-made objects and paved roads. Applying probabilistic fusion to combine multiple data sources, LCCD and SAR RCS for this case, significantly reduces between-class confusion. Because probabilistic fusion models the class of interest and tests for fidelity to the model, it allows an unknown class, which is difficult with many machine learning approaches [53][45][9][43]. Since probabilistic fusion requires p-values to normalize the inputs, the KS test is a natural fit. Its nonparameteric approach allows it to model any distribution from Rayleigh to Weibull to a beta prime distribution. All of which (plus many more) have been proposed to model different types of terrain in SAR images. Unfortunately, the SAR products violate the independence assumption required for the KS test. We have introduced a novel method that uses training data to modify the null distribution, which corrects for dependence between observations in the KS test. This allows the correct p-values to be estimated and the application of probabilistic fusion.

10. Future Work

An obvious extension to this work is to use the same approach for identifying other static-features such as shadow, man-made objects, trees, scrub desert, etc. The probabilistic fusion frame work with the KS test can be easily extended to other static-features and incorporate different SAR products such as polarmeteric SAR. We would also like to apply a conditional random field using the superpixels as the nodes [15] of the graph and the output of the probabilistic fusion algorithm for the unary energy function. This will help improve the segmentation by enforcing spatial consistency constraints.

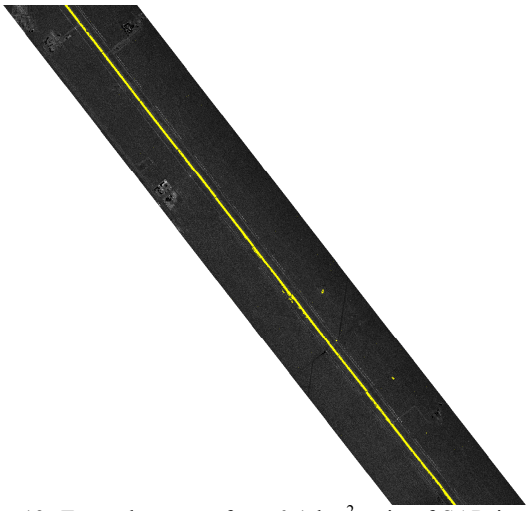

Figure 13: Example output for a 0.1 km^2 strip of SAR imagery. (best viewed in color)).

References

[1] R. Achanta, K. Smith, A. Lucchi, P. Fua, and S. Susstrunk, “SLIC superpixels compared to state-of-the-art superpixel methods,” IEEE Trans. Patt. Anal. and Mach. Intell. 34(11), 2274-2282 (2012).

[2] V. Amberg, M. Coulon, P. Marthon, and M. Spigai, “Improvement of road extraction in high resolution SAR data by a context-based approach,” in Proceedings of the IEEE International Geoscience and Remote Sensing Symposium (IGARSS '05), pp. 490–493, Seoul, Korea, July 2005.

[3] G. V. Bayley and J. M. Hammersley, "The Effective Number of Independent Observations in an Autocorrelated Time Series," *Supplement to the Journal of the Royal Statistical Society*, vol. 8, pp. 184-197, 1946.

[4] R. C. Brost, W. C. McLendon III, O. Parekh, M. D. Rintoul, D. R. Strip, and D. M. Woodbridge, “A computational framework for ontologically storing and analyzing very large overhead image sets,” 3rd ACM SIGSPATIAL International Workshop on Analytics for Big Geospatial Data (BigSpatial-2014), November 2014.

[5] J. Cheng, Y. Guan, X. Ku, and J. Sun, “Semi-automatic road centerline extraction in high-resolution SAR images based on circular template matching,” in Proceedings of the International Conference on Electric Information and Control Engineering (ICEICE '11), pp. 1688–1691, Wuhan, China, April 2011.

[6] J. Cheng, W. Ding, X. Ku, and J. Sun, “Road Extraction from High-Resolution SAR Images via Automatic Local Detecting and Human-Guided Global Tracking,” International Journal of Antennas and Propagation, vol. 2012.

[7] S.R. Cloude, *Polarisation: Applications in Remote Sensing*, Chapter 2, Oxford University Press, 2010.

[8] S.R. Cloude and E. Pottier, “An entropy based classification scheme for land applications of polarimetric SAR,” *Geoscience and Remote Sensing, IEEE Transactions on*, vol. 35, no. 1, pp. 68-78, 1997.

[9] C. Corte and V. Vapnik, "Support-vector networks," *Machine Learning* 20 (3): 273, 1995.

[10] T. R. Crimmins, "Geometric filter for speckle reduction," *Applied Optics*, vol. 24, no. 10, pp. 1438-1443, May 1985.

[11] Y. Cui, Y. Yamaguchi, J. Yang, H. Kobayashi, S. Park G. Singh, “On complete model-based decomposition of polarimetric SAR coherency matrix data,” *Geoscience and Remote Sensing, IEEE Transactions on*, vol. 52, no. 4, pp. 1991-2001, 2014.

[12] R. O. Duda, P. E. Hart, and D. G. Stork, *Pattern classification*, John Wiley & Sons, New York, NY (2012).

[13] M. Evans, N. Hastings, and B. Peacock, Statistical Distributions, John Wiley & Sons, NY, 1993.

[14] V. S. Frost, J. A. Stiles, K. S. Shanmugan, and J. C. Holtzman, "A Model for Radar Images and its Application for Adaptive Digital Filtering of Multiplicative Noise," *IEEE Transactions on Pattern Analysis and Machine Intelligence*, vol. 4, no. 2, pp. 157-165, 1982.

[15] B. Fulkerson, A. Vedaldi, and S. Soatto, “Class segmentation and object localization with superpixel neighborhoods,” Proc. IEEE Comp. Vis., 670-677 (2009).

[16] L. Gagnon and A. Jouan, "Speckle filtering of SAR images: A comparative study beteen complex-wavelet-based and standard filters," *SPIE Proc.*, vol. 3169, pp. 80-91, 1997.

[17] L. Gan, Y. Wu, M. Liu, P. Zhang, H. Ji, and F. Wang, “Triplet Markov fields with edge location for fast unsupervised multi-class segmentation of synthetic aperture radar images,” IET Image Proc. 6(7), 831-838 (2012).

[18] G. Gao, "Statistical modeling of SAR images: A survey." *Sensors* 10, no. 1, pp. 775-795, 2010.

[19] C. He, Z. Liao, F. Yang, X. Deng, and M. Liao, “Road extraction from SAR imagery based on multiscale geometric analysis of detector responses,” IEEE Journal of Selected Topics in Applied Earth Observations and Remote Sensing, vol. 5, no. 5, pp. 1373-1382, 2012.

[20] K. Hedman and S. Hinz, “The application and potential of Bayesian network fusion for automatic cartographic mapping,” in Proceedings of the IEEE International Geoscience and Remote Sensing Symposium (IGARSS '12), pp. 6848–6851, Munich, Germany, July 2012.

[21] K. Hedman, U. Stilla, G. Lisini, and P. Gamba, “Road network extraction in VHR SAR images of urban and suburban areas by means of class-aided feature-level fusion,” IEEE Transactions on Geoscience and Remote Sensing, vol. 48, no. 3, pp. 1294–1296, 2009.

[22] R. Hogg and A. Craig, *Introduction to Mathematical Statistics*, Macmillan, NY, 1978.

[23] C. V. Jakowatz, Jr., D. E.Wahl, P. E. Eichel, D. C. Ghiglia, and P. A.Thompson. *Spotlight-mode Synthetic Aperture Radar: A Signal Processing Approach*. Springer, 1996.

[24] B. Jeon, J. Jang, and K. Hong, “Road detection in spaceborne SAR images using a genetic algorithm,” IEEE Transactions on Geoscience and Remote Sensing, vol. 40, no. 1, pp. 22-29, 2002.

[25] T. Kim, S. R. Park, M. G. Kim, S. Jeong, and K. O. Kim, “Tracking road centerlines from high resolution remote sensing images by least squares correlation matching,” Photogrammetric Engineering and Remote Sensing, vol. 70, no. 12, pp. 1417–1422, 2004.

[26] A. Kolmogorov, “Sulla determinazione empirica di una legge di distribuzione,” *G. Ist. Ital. Attuari,* **4**: 83–91, 1933.

[27] D. T. Kuan, A. A. Sawchuk, and P. Chavel, "Adaptive Restoration of Images with Speckle," *IEEE Transactions on Acoustics*, vol. ASSP-35, pp. 373-383, 1987.

[28] X. G. Lin, J.X. Zhang, Z.J. Liu, and J. Shen, “Semi-automatic extraction of ribbon roads from high-resolution remotely sensed imagery by cooperation between angular texture signature and template matching,” The International Archives of the Photogrammetry, Remote Sensing and Spatial Information Sciences, vol. 37, pp. 539-544, 2008.

[29] X. Lin, Z. Liu, J. Zhang, and J. Shen, “Combining multiple algorithms for road network tracking from multiple source remotely sensed imagery: a practical system and performance evaluation,” Sensors, vol. 9, no. 2, pp. 1237–1258, 2009.

[30] G. Lisini, C. Tison, F. Tupin, and P. Gamba, “Feature fusion to improve road network extraction in high-resolution SAR images,” IEEE Geoscience and Remote Sensing Letters, vol. 3, no. 2, pp. 217–221, 2006.

[31] J. S. Lee, "Speckle Analysis and Smoothing of Synthetic Aperture Radar Images," *Computer Graphics and Image Processing*, vol. 17, pp. 24-32, 1981.

[32] J. S. Lee and T. L. Ainsworth, "The effect of orientation angle compensation on coherency matrix and polarimetric target decompositions," *Geoscience and Remote Sensing, IEEE Transactions on*, vol. 49, no. 1, pp. 53-64, 2011.

[33] J. S. Lee and I. Jurkevich, "Segmentation of SAR Images," IEEE Transactions on Geoscience and Remote Sensing," vol. 27, 6, November 1989.

[34] J. S. Lee and E. Pottier, *Polarimetric Radar Imaging: From Basics to Applications*, Chapter 7, CRC Press, 2002.

[35] A. Levinshtein, A. Stere, K. N. Kutulakos, D. Fleet, S. J. Dickinson, and K. Siddiqui, "Turbopixels: Fast superpixels using geometric flows," IEEE Trans. Patt. Anal. and Mach. Intell. 31(12), 2290-2297 (2009).

[36] P. Lu, K. Du, W. Yu, R. Wang, Y. Deng, and T. Balz, "A new region growing-based method for road network extraction and its application on different resolution SAR images," IEEE Journal of Selected Topics in Applied Earth Observations and Remote Sensing, vol. 7, no. 12, pp. 4772-4783, 2014.

[37] S. P. Lloyd, "Least squares quantization in PCM". *IEEE Transactions on Information Theory* 28 (2), pp. 129–137, 1982.

[38] M. M. Moya, M. W. Koch, D. N. Perkins, R. D. West, "Superpixel segmentation using multiple SAR image products," *Radar Sensor Technology XVIII (DS 108), SPIE Defense, Security, and Sensing Symposium* Baltimore, MD, May 6, 2014.

[39] M. Negri, P. Gamba, G. Lisini, and F. Tupin, "Junction-aware extraction and regularization of urban road networks in high-resolution SAR images," IEEE Transactions on Geoscience and Remote Sensing, vol. 44, no. 10, pp. 217–221, 2006.

[40] E. Parzen, "On estimation of probability density function and mode," *Annals of Mathematical Statistics*, 33:1065-1076, 1962.

[41] T. Perciano, F. Tupin, R. Hirata, Jr., and R. Cesar, Jr., "A hierarchical Markov random field for road network extraction and its application with optical and SAR data," in Proceedings of the IEEE International Geoscience and Remote Sensing Symposium (IGARSS '11), pp. 1159–1162, Vancouver, Canada, July 2011.

[42] A. A. Popescu, I. Gavat, and M. Datcu, "Contextual descriptors for scene classes in very high resolution SAR images," IEEE Geoscience and Remote Sensing Letters, vol. 9, no. 1, pp. 80-84, 2012.

[43] W. H. Press, S. A. Teukolsky, W. T. Vetterling, and B. P. Flannery, *Numerical Recipes 3rd Editions: The Art of Scientific Computing*, Cambridge University Press, pp. 736-738, 2007.

[44] X. Ren and J. Malik, "Learning a classification model for segmentation," Proc. IEEE Comp. Vis. 1, 13-16 (2003).

[45] D. E. Rumelhart and J. McClelland, *Parallel Distributed Processing: Explorations in the Microstructure of Cognition*. Cambridge: MIT Press, 1986.

[46] J. S. Salazar, *Detection Schemes for Synthetic Aperture Radar Imagery Based on a Beta Prime Statistical Model*, PhD Dissertation, New Mexico University, Albuquerque, NM, 1999.

[47] J. S. Salazar, J.S., "Statistical modeling of target and clutter in single-look non-polorimetric SAR imagery," *Proceedings of International Conference Signal and Image Processing*, Las Vegas, CA, USA, October 1998.

[48] K. Simonson, "Probabilistic fusion of ATR results," Sandia Report, SAND98-1699, August 1998.

[49] G. Singh, Y. Yamaguchi and S.E. Park, "General four-component scattering power decomposition with unitary transformation of coherency matrix," *Geoscience and Remote Sensing, IEEE Transactions on*, vol. 51, no. 5, pp. 3014-3022, 2013.

[50] N. Smirnov, "Table for estimating the goodness of fit of empirical distributions," Annals of Mathematical Statistics, **19**: 279–281, 1948.

[51] X. Su, C. He, Q. Feng, X. Deng and H. Sun, "A supervised classification method based on conditional random fields with multiscale region connection calculus model for SAR image," IEEE Geosci. and Rem. Sens. Lett. 8(3), 497-501 (2011).

[52] F. T. Ulaby and M. C. Dobson, *Handbook of Radar Scattering Statistics for Terrain*, (Norwood, MA: Atrech House, 1989).

[53] P. J. Werbos, *Beyond Regression: New Tools for Prediction and Analysis in the Behavioral Sciences*, 1975.

[54] B. Wessel, "Road network extraction from SAR imagery supported by context information," The International Archives of the Photogrammetry, Remote Sensing and Spatial Information Sciences, vol. 35, pp. 360-366, 2004.

[55] Y. Wu, X. Wang, P. Xiao, L. Gan, C. Y. Liu, and M. Li, "Fast algorithm based on triplet Markov fields for unsupervised multi-class segmentation of SAR images," Sci. China Info. Sci. 54(7), 1524-1533 (2011).

[56] D. Xiang, T. Tao, Z. Lingjun, and S. Yi,, "Superpixel generating algorithm based on pixel intensity and location similarity for SAR image classification," IEEE Geosci. and Rem. Sens. Lett. 10(6), 1414-1418 (2013).

[57] Y. Yamaguchi, T. Moriyama, M. Ishido, and H Yamada, "Four-component scattering model for polarimetric SAR image decomposition," *Geoscience and Remote Sensing, IEEE Transactions on*, vol. 43, no. 8, pp. 1699-1706, 2005.

[58] Y. Yang and C. Zhu, "Extracting road centrelines from high-resolution satellite images using active window line segment matching and improved SSDA," International Journal of Remote Sensing, vol. 31, no. 10, pp. 2457–2469, 2010.

[59] H. Yu, X. Zhang, S. Wang, and B. Hou, "Context-Based Hierarchical Unequal Merging for SAR Image Segmentation," IEEE Trans. Geosci. and Rem. Sens. 51(2), 995-1009 (2013).

[60] J. Zhang and Y. Wu, "Beta approximation to the distribution of the Kolmogorov-Smirnov statistic," Ann. Inst. Statist. Math., Vol. 54, No. 3, 577-584, 2002.